CSIRO Publishing

Publications of the Astronomical Society of Australia

VOLUME 18, 2001

An international journal of astronomy and astrophysics

For editorial enquiries and manuscripts, please contact:
The Editor, PASA,
ATNF, CSIRO,
PO Box 76,
Epping, NSW 1710, Australia
Telephone: +61 2 9372 4590
Fax: +61 2 9372 4310
Email: Michelle.Storey@atnf.csiro.au

For general enquiries and subscriptions, please contact:
CSIRO Publishing
PO Box 1139 (150 Oxford St)
Collingwood, Vic. 3066, Australia
Telephone: +61 3 9662 7666
Fax: +61 3 9662 7555
Email: pasa@publish.csiro.au

Published by CSIRO Publishing
for the Astronomical Society of Australia

www.publish.csiro.au/journals/pasa

https://doi.org/10.1071/AS01041 Published online by Cambridge University Press

Publ. Astron. Soc. Aust., 2001, 18, 232–242

FLAIR II Spectroscopy of Two DENIS J Band Galaxy Samples

Gary A. Mamon[1,2], Quentin A. Parker[3,4] and Dominique Proust[2]

[1]Institut d'Astrophysique de Paris, 98 bis Bd Arago, F–75014 Paris, France
gam@iap.fr
[2]DAEC, Observatoire de Paris, F–92195 Meudon, France
[3]Institute for Astronomy, Royal Observatory, Edinburgh, United Kingdom
[4]Anglo-Australian Observatory, Coonabarabran, NSW 2357, Australia

Received 2001 March 2, accepted 2001 July 14

Abstract: As a pilot survey for the forthcoming 6dF Galaxy Redshift Survey, spectroscopy of galaxies selected in the 1.2 micron J waveband with the DENIS imaging survey was performed at the UKST using the FLAIR II multi-object spectroscope. Sixty-nine galaxy redshifts were obtained in a high galactic latitude field and an additional 12 redshifts in a low galactic latitude ($b = -17°$), obscured field. This spectroscopic followup of NIR selected galaxies illustrates the feasibility of obtaining redshifts with optical spectra on galaxies selected at much longer wavelengths. It validated a very preliminary algorithm for star/galaxy separation for high galactic latitude DENIS objects, with 99% reliability for $J < 13.9$. The FLAIR II redshifts are in excellent agreement with those, previously published, of 20 common galaxies. However, the FLAIR II redshift determinations presented here required substantially longer integration times to achieve 90% completeness than expected from previous optical surveys at comparable depth. This is mainly due to a degradation in overall fibre throughput due to known problems with ageing of the prism–cement–fibre interface with exposure to UV light. In comparison to our high galactic latitude field, our low latitude (high extinction) field required 2.5 times more exposure time for less than 50% of successful redshift measurements.

Among the $J \leq 13.9$ galaxies with measured redshifts, only 37 ± 6% display emission lines, in comparison with 60% of emission line galaxies in optical samples of comparable depth. These galaxies are, on average, half a magnitude bluer in $B - J$ than galaxies of the same luminosity without emission lines. We confirm a previous optically-based result that the fraction of galaxies with emission lines increases rapidly with decreasing galaxy luminosity. The J band luminosity function is estimated. Our high latitude field displays a concentration of galaxies at $cz \simeq 38\,000\,\mathrm{km\,s^{-1}}$ suggesting a possible supercluster. A radial velocity is reported for a galaxy lying near the projected centre of the Abell 1434 cluster of galaxies, for which no cluster redshift is currently available.

Keywords: infrared: galaxies — cosmology: observations — surveys — galaxies: luminosity function

1 Introduction

The recent advances in detector technology in the near infrared (hereafter NIR) domain have brought much enthusiasm to the field of large-scale structure of the universe. Indeed, NIR light has the strong advantage of being much less affected by extinction from dust grains than is optical light, and as such, NIR galaxy images show spiral galaxies in a much simpler light, traced by their old stellar populations, with little dust obscuration in spiral arms and in the galaxy centres (Zaritsky, Rix & Rieke 1993; Héraudeau, Simien & Mamon 1996). Moreover, NIR emission is less affected by recent bursts of star formation within a galaxy, that can result in relatively small numbers of new hot OB stars contributing a substantial fraction of the optical light of the entire galaxy. Finally, the transparency of dust grains to NIR photons means that our own Galaxy will not obscure the view of external galaxies imaged in the NIR. However, within a few degrees from the Galactic plane, confusion from stars sets in and prevents reliable star/galaxy separation (e.g. Jarrett et al. 2000b).

For these reasons, tracing the distribution of mass in the universe with galaxies becomes much more meaningful if the galaxies are selected in the NIR domain. Two very large NIR digital imaging surveys, DENIS (e.g. Epchtein et al. 1999) and 2MASS (e.g. Jarrett et al. 2000a), are producing galaxy catalogues that are essential for such cosmological studies in two dimensions. Moreover, there is much science to be gained by using redshifts to give a third dimension. With this in mind, we have approval to use the soon to be commissioned 6dF robotic multi-fibre spectroscope (Parker, Watson & Miziarski 1998; Watson et al. 2000) on the UKST to undertake the massive 6dF Galaxy Redshift Survey (hereafter 6dFGRS, e.g. Mamon 1998; 1999; see also `http://msowww.anu.edu.au/~colless/6dF`) of roughly 120 000 galaxies selected from 2MASS and DENIS. This large survey is scheduled to begin in the southern autumn of 2001.

In a pilot study of 6dFGRS, we tested the feasibility of measuring redshifts with optical spectroscopy of NIR selected galaxy samples. For this, we observed two Schmidt plate sized fields of galaxies, selected in the J (1.25 μm) band with early DENIS observations. The spectroscopy was performed at the UKST with the FLAIR II multi-fibre instrument (e.g. Parker & Watson 1995), which

10.1071/AS01041 1323-3580/01/03232$05.00

has now been decommissioned pending the introduction of the automated 6dF. The results of this pilot study are reported in the present paper.

2 Sample Selection

Galaxies were selected from preliminary DENIS extractions performed during February 1998, with a galaxy pipeline, based upon SExtractor (Bertin & Arnouts 1996) and a simple preliminary star/galaxy separation algorithm based upon a threshold of the ratio of peak intensity to isophotal area (I/A), which, to first order, does not depend on magnitude (Mamon et al. 1998). This star/galaxy separation is performed in the DENIS I band, which is much more sensitive and has better spatial resolution than the DENIS J or K bands. The target galaxy samples were taken from the contiguous DENIS strips that overlap regions of UKST standard survey fields F787 (12h00, $-5°$) at high galactic latitude ($b = 55°$), and F20 (12h00, $-80°$) at low galactic latitude ($b = -17°$).

All objects in DENIS *strips* of 180 consecutive images at constant RA crossing these fields, with $J \leq 13.9$, and below *or slightly above* the star/galaxy separation (I/A) threshold (which depends on the DENIS strip), were selected. The J photometry is based upon the Kron (1980) estimator of the total flux of galaxies. The internal photometric errors, based upon multiple observations of single objects, are $\Delta J \simeq 0.10$ at $J = 13.7$ (Mamon et al. 1998). We made use of an early photometric calibration that is estimated to be accurate to better than 0.2 magnitude.

Note that our samples do not provide full coverage of the two UKST fields, as only a fraction of DENIS strips (11 out of 30 for field F787 and 5 out of 27 for field F20) had been observed at the time of the observations. We ended up with 87 candidate objects in field F787, of which 84 were below the star/galaxy separation threshold. Field F20 turned out to be heavily obscured by the Chameleon cloud, and only 33 objects were extracted, all above the star/galaxy separation threshold (i.e. as galaxies according to DENIS).

We did not target objects that were obvious stars, as well as objects that lay close to others, because of constraints on the minimum fibre separation, leaving us with 78 targeted objects in field F787 and 32 objects in field F20.

For all objects, B magnitudes were extracted from the ROE/NRL UKST COSMOS Catalogue (hereafter COSMOS).[1] The cross-identification was performed with a $6''$ search radius for galaxies in astrometrically calibrated DENIS strips (strip number greater than 5000), and with a $30''$ search radius otherwise. In nearly all cases, the DENIS and COSMOS astrometries matched to within $3''$ (even among the non-calibrated DENIS images). All cases with no matches within $3''$ were inspected visually on DENIS and Digitized Sky Survey (hereafter, DSS) images. In field F787, six objects had astrometric matches within $5''$ to $12''$. In field F20, one object with no astrometric match turned out to be a false DENIS detection, a ghost caused by a nearby very bright and saturated star. Three objects had COSMOS counterparts within $5''$ to $10''$ and one object had its COSMOS counterpart at $69''$. Comparison with the DSS showed that the astrometric offsets were caused by the lack of calibration of many of the DENIS images. In particular, the mismatch of $69''$ was caused by the poor telescope pointing due to large camera flexure at the end of a polar DENIS strip, with the telescope operating at large zenith angle.

3 Observations and Data Reduction

The spectroscopic observations were performed with the FLAIR II 92-fibre spectrograph at the UKST at Siding Spring. The telescope has a 1.24 m diameter aperture, and uses $6''.7$ fibres. We made use of the low spectral resolution 250B grating, with a spectral resolution of 6.14 Å/pixel, observing in the spectral range 4180 Å–7726 Å. The spectrograph is described in detail in Parker & Watson (1995).

The fibres of the plate-holders were configured, off telescope, during daytime, with about 11 fibres reserved for sky background measurements to facilitate sky subtraction.

Out of the seven allocated nights, we were only able to observe two fields with the FLAIR II spectrograph because of intermittent cloud cover. The details of the observations are given in Table 1. For field F787, we measured the radial velocities on data taken in a batch of 4200 s and in a longer batch of 17 400 s including the previous one,[2] while for field F20, we only attempted redshift measurements on a long batch of 44 200 s. Sky-subtracted, spectrally calibrated spectra were obtained by reducing the data as in Ratcliffe et al. (1998), using the `dofibers` package in IRAF. In particular, dome and twilight flats were used. Spectral calibration was performed with HgCd arcs. Glitches were removed. After some experimentation, we combined different exposures by scaling to their exposure times.

The redshifts were obtained as follows. For absorption-featured spectra, redshifts were obtained using the cross-correlation task XCSAO in the RVSAO package (Kurtz & Mink 1998) within IRAF, using a series of template spectra from stars, absorption line and emission line galaxies. We decided to adopt as the absorption velocity the one associated with the minimum error from the cross-correlation against the templates. In the great majority of cases, this coincided also with the maximum R parameter of Tonry & Davis (1979). The redshifts for the emission line objects were determined using the EMSAO task in RVSAO. EMSAO finds emission lines automatically, computes redshifts for each identified line and combines

[1] See `http://xip.nrl.navy.mil/www_rsearch/RS_form.html`

[2] Visual inspection of the spectra suggests that the two batches have signal-to-noise ratios proportional to the square root of their respective exposure times, to within 10–20%.

https://doi.org/10.1071/AS01041 Published online by Cambridge University Press

them into a single radial velocity with error. Spectra showing both absorption and emission features were generally measured with the two tasks XCSAO and EMSAO and the result with the lower error used.

4 Results

4.1 Redshifts

We measured velocities successfully for 70 objects in field F787 and 13 objects in field F20. One object in field F787 at $v = 500\,\mathrm{km\,s^{-1}}$ looks like an M star from apparent TiO absorption bands, and one object in field F20 was also a star ($v = -6\,\mathrm{km\,s^{-1}}$). The results for the 81 spectroscopically confirmed galaxies are presented in Tables 2 and 3 for fields F787 and F20, respectively.

For the 20 galaxies of field F787 that have spectroscopic redshifts available in the NED database, we have

$$v_{\mathrm{FLAIR}} = v_{\mathrm{NED}} - 49 \pm 74\,\mathrm{km\,s^{-1}}.$$

Unsurprisingly, there are no redshifts in the low galactic latitude field F20 present in the NED database.

4.2 Reliability of the Preliminary DENIS Galaxy Pipeline

Among the 87 objects extracted by DENIS in field F787, all but two appeared as galaxies upon visual inspection of the UKST photographic plate, while two appeared star-like. These two stellar objects were classified as stars by DENIS. Note that the third object classified as a star by

Table 1. Journal of FLAIR II observations

Date	Field	RA (B1950)	Dec (B1950)	Grating	Exposure	Seeing	Weather
1998 March 1	F787	12h00m00s	−05°00′00″	250B	17 400 s	2−3″	cloud
1998 March 4	F20	12h00m00s	−80°00′00″	250B	21 500 s	1−2″	cloud
1998 March 6	F20	12h00m00s	−80°00′00″	250B	8 200 s	2−3″	cloud
1998 March 7	F20	12h00m00s	−80°00′00″	250B	14 500 s	2−4″	cloud

Table 2. Galaxy redshifts in field F787

Id	RA (J2000)	Dec (J2000)	COSMOS type	b_J	DENIS strip	J	v ($\mathrm{km\,s^{-1}}$)	δv ($\mathrm{km\,s^{-1}}$)	R	Cont.	Spec. type
F787–01	11h52m17.6s	–07d05m24.0s	G	17.60	4039	13.88	19604	118	4.5	105	abs
F787–02	11h52m28.0s	–04d26m28.1s	G	16.91	3708	13.29	24315	117	4.4	125	abs
F787–03	11h52m38.0s	–05d12m25.6s	G	14.78	5570	11.60	5641	23	26.1	310	em
F787–04	11h52m42.5s	–05d04m36.2s	G	17.70	4062	12.74	14675	36	6.9	240	abs
F787–05	11h52m59.7s	–04d25m36.0s	G	14.14	3882	12.66	1447	71	10.0	170	em
F787–06	11h53m00.7s	–04d52m45.3s	G	17.02	5436	13.40	19676	74	4.6	55	abs
F787–07	11h53m01.1s	–06d03m54.4s	G	15.94	3905	12.57	6584	45	9.1	470	abs
F787–08	11h53m02.4s	–07d37m30.9s	G	15.33	4031	13.07	7179	64	13.7	180	em
F787–09	11h53m40.5s	–03d59m46.3s	G	13.84	3882	11.90	1545	73	10.8	215	em
F787–10	11h53m44.6s	–05d25m35.9s	G	15.92	4024	12.41	5779	36	9.9	480	abs
F787–11	11h53m48.7s	–05d10m04.2s	G	13.84	3905	10.84	5682	78	8.8	440	em
F787–12	11h53m59.0s	–02d47m31.5s	G	17.18	4031	13.66	26885	126	2.7	80	abs
F787–13	11h54m00.9s	–06d12m30.7s	G	17.10	3882	13.89	5493	69	12.1	130	abs
F787–14	11h54m04.8s	–05d49m59.8s	G	17.56	5570	13.77	17188	71	7.4	155	em
F787–15	11h55m00.9s	–06d05m20.9s	G	15.08	5431	11.53	7741	58	7.5	770	em
F787–16	11h55m10.2s	–07d50m37.0s	G	14.37	4031	11.00	5588	32	9.6	1750	abs
F787–17	11h55m17.9s	–03d43m34.8s	G	17.67	4039	13.90	19020	59	3.6	60	abs
F787–18	11h55m35.0s	–04d48m43.0s	G	16.18	4039	13.38	18489	76	3.7	160	em
F787–19	11h56m07.9s	–05d45m41.1s	G	16.36	3708	12.83	16938	33	9.4	500	abs
F787–20	11h56m12.2s	–05d28m59.4s	G	17.15	5436	13.58	24605	69	6.3	190	abs
F787–21	11h56m13.7s	–03d40m17.0s	S	13.16	3905	13.18	6395	75	5.0	140	em
F787–22	11h56m29.1s	–06d24m56.3s	G	16.41	5436	12.81	14937	27	5.4	210	abs
F787–23	11h56m43.0s	–07d24m33.8s	G	16.49	5436	13.84	10654	78	2.3	160	abs
F787–24	11h56m47.6s	–05d08m06.3s	G	17.35	4031	13.88	20070	109	4.3	70	abs
F787–25	11h56m48.5s	–04d05m40.6s	G	15.20	3708	11.18	7845	30	10.6	800	abs
F787–26	11h57m00.1s	–07d13m13.9s	G	17.20	3882	13.67	11119	49	9.0	300	abs
F787–27	11h59m14.4s	–04d05m46.2s	G	16.37	4031	11.39	14128	52	5.2	155	abs
F787–28	11h59m23.6s	–03d49m30.5s	G	16.13	3905	12.78	9508	62	3.3	100	abs
F787–29	11h59m24.5s	–06d44m12.1s	G	15.85	5431	12.17	8705	32	7.8	500	abs
F787–30	11h59m35.2s	–06d53m52.6s	G	17.46	3905	13.62	37954	69	7.2	125	abs

https://doi.org/10.1071/AS01041 Published online by Cambridge University Press

Table 2. (*Continued*)

Id	RA (J2000)	Dec (J2000)	COSMOS type	b_J	DENIS strip	J	v (km s^{-1})	δv (km s^{-1})	R	Cont.	Spec. type
F787–31	11h59m35.2s	–06d39m44.3s	G	17.57	5415	13.92	22016	104	5.3	210	abs
F787–32	11h59m35.6s	–07d13m47.8s	G	16.08	4031	13.03	15442	64	9.4	380	em
F787–33	11h59m36.2s	–06d49m35.2s	S	14.35	4039	13.83	38514	25	5.7	180	abs
F787–34	11h59m38.3s	–03d22m39.1s	G	16.67	3905	13.15	5829	81	6.2	170	abs
F787–35	11h59m38.9s	–03d40m55.8s	G	15.47	3882	12.27	5856	73	0.0	320	em
F787–36	11h59m43.9s	–05d46m05.0s	G	17.70	5431	13.96	18823	30	6.3	120	abs
F787–37	12h00m18.4s	–07d10m51.2s	G	15.54	4024	12.12	20572	63	10.3	310	abs
F787–38	12h00m18.4s	–04d11m36.7s	G	16.99	3905	13.92	15760	82	5.3	70	em
F787–39	12h00m37.8s	–06d51m21.2s	G	17.71	5570	13.74	38055	33	7.4	260	abs
F787–40	12h00m41.1s	–05d45m53.0s	G	16.71	4024	13.67	7843	57	13.8	120	em
F787–41	12h02m23.0s	–03d18m22.5s	G	16.76	5415	13.09	20283	94	3.3	45	abs
F787–42	12h02m25.6s	–04d18m21.7s	G	15.32	3882	12.82	5639	55	9.7	115	em
F787–43	12h02m45.2s	–03d47m20.8s	G	17.25	5570	13.73	19355	95	3.3	135	em
F787–44	12h02m52.7s	–06d48m21.8s	G	17.87	4039	13.84	38707	84	4.2	120	abs
F787–45	12h02m58.4s	–06d50m45.5s	G	17.35	3905	13.55	38524	55	4.3	170	abs
F787–46	12h03m38.2s	–06d48m46.3s	G	17.12	4024	13.73	15723	129	3.6	95	abs
F787–47	12h03m51.2s	–04d03m11.9s	G	17.97	4039	13.78	39454	117	4.7	50	abs
F787–48	12h03m53.3s	–07d51m39.7s	G	16.93	3708	13.25	19152	43	7.6	300	abs
F787–49	12h03m54.7s	–06d32m20.4s	G	16.29	4031	13.44	1754	66	9.0	70	em
F787–50	12h04m16.5s	–07d10m08.5s	G	18.01	3905	13.92	55087	58	5.9	190	abs
F787–51	12h04m23.0s	–05d17m47.6s	G	15.04	5436	11.65	8032	83	16.0	700	em
F787–52	12h04m23.7s	–07d44m32.6s	G	17.51	3882	13.67	20908	194	2.6	65	abs
F787–53	12h04m58.9s	–05d34m53.0s	G	16.91	4024	13.90	7928	59	7.8	90	em
F787–54	12h05m00.5s	–05d52m53.1s	G	16.90	5570	13.54	16730	83	4.5	195	abs
F787–55	12h05m07.1s	–04d04m53.5s	G	16.57	5431	12.94	9259	65	7.8	180	abs
F787–56	12h05m07.8s	–04d12m36.1s	G	16.59	5431	13.69	14067	50	5.4	90	em
F787–57	12h05m12.3s	–03d54m14.4s	G	14.81	5570	11.41	5604	64	6.5	370	abs
F787–58	12h05m15.0s	–06d51m18.3s	G	15.63	4062	13.44	7770	35	10.0	215	em
F787–59	12h05m27.7s	–04d16m05.8s	G	16.12	4031	12.63	9189	82	10.4	110	em
F787–60	12h05m25.8s	–04d24m42.5s	S	14.26	5431	13.75	24227	46	5.1	290	em
F787–61	12h05m31.9s	–07d38m25.9s	G	17.08	3882	13.45	20937	42	5.9	205	abs
F787–62	12h05m33.1s	–04d30m23.0s	G	16.95	5436	13.42	24428	111	3.9	130	abs
F787–63	12h05m34.3s	–06d46m18.1s	G	17.51	5415	13.96	41359	137	3.1	125	abs
F787–64	12h05m39.0s	–07d05m28.9s	G	17.78	4062	13.94	37682	84	6.8	220	abs
F787–65	12h06m37.6s	–06d33m40.3s	G	16.62	3882	13.70	23139	52	0.0	210	em
F787–66	12h06m40.6s	–04d26m21.5s	G	17.45	3882	13.87	25298	44	8.7	100	abs
F787–67	12h06m43.4s	–04d55m12.2s	G	17.14	5431	13.55	32250	150	3.3	55	abs
F787–68	12h06m55.4s	–07d08m23.6s	G	16.72	4062	13.77	18670	90	4.8	95	em
F787–69	12h07m03.5s	–04d20m51.1s	G	17.24	5570	13.45	24678	81	7.8	210	abs

Notes: The astrometry is taken from COSMOS. 'COSMOS type' is 'G' for galaxy and 'S' for star; v is the measured radial velocity and δv is its uncertainty; R is the Tonry & Davis (1979) correlation parameter; 'Cont.' gives the maximum continuum, typically reached around 5500 Å, in arbitrary units; 'spec. type' gives the spectral type: 'em' for the presence of emission lines, otherwise 'abs' (for absorption lines only). Visual inspection of the photographic UKST plates and cross-identification with NED indicated the following:

F787–05 = VV 457.
F787–09 = NGC 3952.
F787–14 is a binary galaxy.
F787–16 = NGC 3967.
F787–35 has a star superposed on the galaxy.
F787–37 is within 42″ of the cluster Abell 1434.
F787–49 is a low surface brightness galaxy.
F787–61 is a galaxy triplet.

DENIS turned out to be a galaxy upon visual inspection of the UKST plate. Hence, from visual inspection, the DENIS galaxy extraction was 100% reliable, but incomplete. Among the 85 visually classified galaxies, 78 were targeted with FLAIR. The resultant spectra produced 69 galaxy redshifts, one stellar spectrum and eight spectra for which no redshift could be determined. In particular, all three galaxies that DENIS found to be very close to the star/galaxy separation threshold were targeted and spectroscopically confirmed as galaxies.

In any event, the reliability of the DENIS galaxy extraction for the high latitude field F787 is between $69/78 = 88\%$ and $68/69 = 99\%$, with a preference for the higher value, given the visual classifications.

In comparison, four of the 84 DENIS candidate galaxies of field F787, as well as the galaxy (from visual inspection) that was classified as stellar by DENIS were associated with stars according to COSMOS. Each of these five COSMOS 'stars' appeared like galaxies upon visual inspection of the photographic plate, and subsequent

https://doi.org/10.1071/AS01041 Published online by Cambridge University Press

Table 3. Galaxy redshifts in field F20

Id	RA (J2000)	Dec (J2000)	COSMOS type	b_J	DENIS strip	J	v (km s^{-1})	δv (km s^{-1})	R	Cont.	Spec. type
F20–01	11h20m54.0s	–78d44m30.6s	G	17.72	3674	13.21	4974	35	5.1	250	em
F20–02	11h21m06.3s	–78d25m02.1s	G	16.46	3674	12.48	11508	42	9.9	800	em
F20–03	11h21m59.4s	–80d21m26.5s	G	17.52	3674	13.58	11467	96	3.5	170	abs
F20–04	11h23m50.7s	–79d58m34.8s	G	18.04	3674	13.56	23328	41	4.8	280	abs
F20–05	11h25m01.6s	–79d31m35.8s	G	18.25	3674	13.70	21779	67	2.8	400	abs
F20–06	11h28m36.3s	–78d17m53.0s	G	17.84	3988	13.69	18805	12	9.9	480	em
F20–07	11h29m22.7s	–80d36m30.9s	G	16.69	3988	13.43	22798	92	2.7	205	abs
F20–08	11h53m38.8s	–78d56m24.2s	G	16.80	3628	13.37	12124	43	9.9	500	em
F20–09	11h53m57.0s	–80d42m07.1s	G	17.87	3628	13.42	13163	91	5.3	480	abs
F20–10	12h02m30.9s	–81d15m03.3s	G	17.83	3701	13.74	13549	123	3.7	180	abs
F20–11	12h04m02.1s	–78d49m54.2s	G	17.36	3701	13.68	21229	18	9.9	500	em
F20–12	12h08m44.4s	–78d45m43.5s	G	17.97	3624	12.49	29692	62	6.1	570	abs

Notes: Columns are the same as in Table 2.

checks with DENIS and DSS images. Three of these five COSMOS 'stars' were spectroscopically confirmed as galaxies (objects F787–21, F787–33, F787–60), while one did not produce a redshift and one was not targeted. All five of these COSMOS 'stars' visually identified as galaxies had very bright COSMOS magnitudes ($b_J < 15$), given their J magnitudes, i.e. they appeared very blue. Systematic flux overestimates and stellar classifications of bright galaxies by COSMOS have already been noted in a systematic comparison with DENIS (Mamon 2000).

Among the 33 objects extracted by DENIS in the low galactic latitude field F20, inspection of the UKST photographic plate indicated that two were stars,[3] one was too faint to classify, and one had no counterpart (a ghost,[4] see end of Section 2). Finally one object had poor astrometry (see end of Section 2) and turned out to be the same galaxy as another. This yields a visually estimated reliability of $28/31 = 90\%$. All but one of the 30 objects that did not appear as stars nor the ghost were targeted with FLAIR II. Among the 29 spectra, 12 were spectroscopically classified as galaxies, one as a star, and 17 produced no redshift. Thus, the reliability of the DENIS galaxy extraction for the low latitude field F20 is between $12/29 = 41\%$ and $12/13 = 92\%$, again with a preference for the higher value, based upon visual classification.

In comparison, COSMOS classified as stars three of the 33 galaxies, among which the two visually classified stars that were not targeted with FLAIR II. The remaining COSMOS 'star' produced no redshift.

Note that the two objects with stellar spectra (one in field F787 and one in field F20) were both classified as galaxies by DENIS and COSMOS, and appeared as galaxies by visual inspection of the UKST plate and the DENIS image, and we suspect that the stellar spectra were caused by incorrect fibre configurations.

[3]The current DENIS pipeline would reject these objects for being too close to one of the edges of their image.
[4]Such ghosts are filtered by the current DENIS pipeline.

4.3 Efficiency of FLAIR II

For field F787, among the nominal 92 FLAIR II fibres, 11 were targeted at the sky, while three were broken, leaving a total of 78 object fibres. For our long batch of 17 000 s of FLAIR II observations, we successfully measured 70 redshifts out of 78 candidates, among which 69 were galaxies. Among the eight failures, we suspect that one or two fibres were improperly configured.

Table 4 summarises the numbers and fractions of successful redshift measurements for 4000 s and 17 000 s exposures in the high latitude F787 field. At the limiting magnitude of our survey ($J \leq 13.9$), we obtained redshifts for 2/3 of our galaxy sample for 4 ks exposures and for 90% of our sample for 17 ks exposures.

Figure 1 illustrates the success and failure of redshift measurements in field F787, using 4000 s and 17 000 s exposures. The galaxies close to the J band limiting magnitude are much redder than average, but still allow for redshift measurements. In fact, we successfully obtained galaxy redshifts in the $17.5 < b_J < 18$ magnitude interval, usually not studied with FLAIR II. The failures for 17 ks exposures are not concentrated in the high b_J region. This can be caused by either poor b_J photometry, as strongly suggested by the failure (cross at [13.7, 14.2] in Figure 1) for a galaxy that is bright in b_J but faint in J.

Figure 2 provides another look at the success rate of redshift determinations, by plotting the maximum continuum versus the J magnitude. The redshift failures are restricted to low continua except for a few galaxies that are faint in J (and in B) with moderate continua.

The large fraction of redshift failures may reflect the strong non-uniformity in the fibre transmissions seen during this run. Indeed, as illustrated in Figure 3, our dome flats indicated fibre transmissions that differed by factors of close to four in the worst cases. Among the eight cases of redshift failure for the 17 000 s exposures, seven were with fibres that had transmission less than half that of the best fibre, and the transmission of the remaining one was lower than 60% of that of the best one. Similarly, for our

https://doi.org/10.1071/AS01041 Published online by Cambridge University Press

Table 4. Redshift success rates for long and short exposures in field F787

$J^{\rm lim}$	N	P(success)		$b_J^{\rm lim}$	N	P(success)	
		17 ks	4 ks			17 ks	4 ks
13.0	22	1.00 ± 0.00	0.86 ± 0.08	16.0	21	0.95 ± 0.05	0.90 ± 0.07
13.3	30	0.97 ± 0.03	0.83 ± 0.07	16.5	30	0.97 ± 0.03	0.87 ± 0.07
13.6	42	0.95 ± 0.03	0.79 ± 0.07	17.0	45	0.93 ± 0.04	0.76 ± 0.07
13.9	70	0.90 ± 0.04	0.67 ± 0.07	17.5	62	0.90 ± 0.04	0.69 ± 0.07
14.2	78	0.88 ± 0.04	0.65 ± 0.07	18.0	77	0.88 ± 0.04	0.65 ± 0.07

Notes: $J^{\rm lim}$ and $b_J^{\rm lim}$ are limiting magnitudes in the NIR J and optical b_J wavebands, respectively. N represents the total number of targeted objects within the given limiting magnitude. P(success) is the probability of successful galaxy redshift measurement, i.e. the fraction of targeted objects that led to non-stellar redshifts. The error bars are binomial.

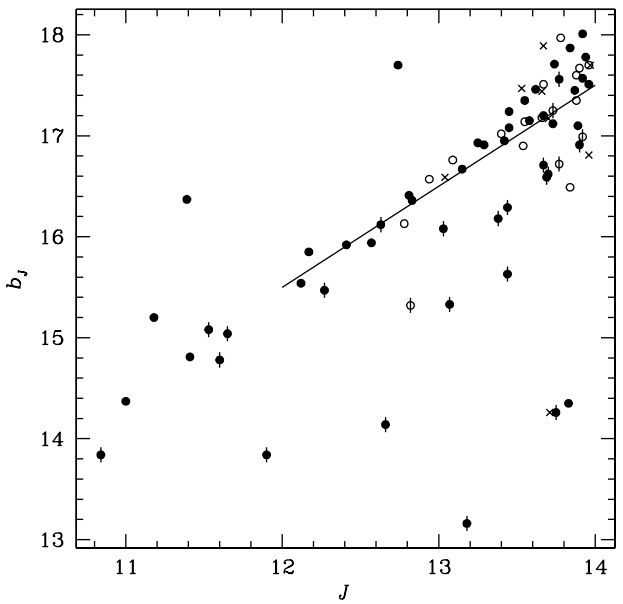

Figure 1 Optical versus NIR magnitude for galaxies, distinguished by the success of redshift measurements (field F787). *Full circles*: redshifts obtained in 4000 s. *Open circles*: redshifts obtained in 17 000 s but not in 4000 s. *Crosses*: redshifts not obtained in 17 000 s. *Circles with vertical bars*: galaxies with emission lines. The line indicates a constant colour $b_J - J = 3.5$.

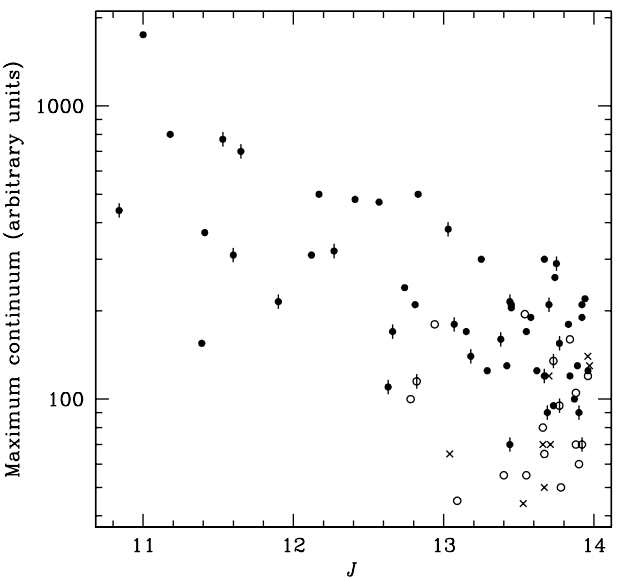

Figure 2 Maximum continuum versus J magnitude for field F787. Same symbols as in Figure 1.

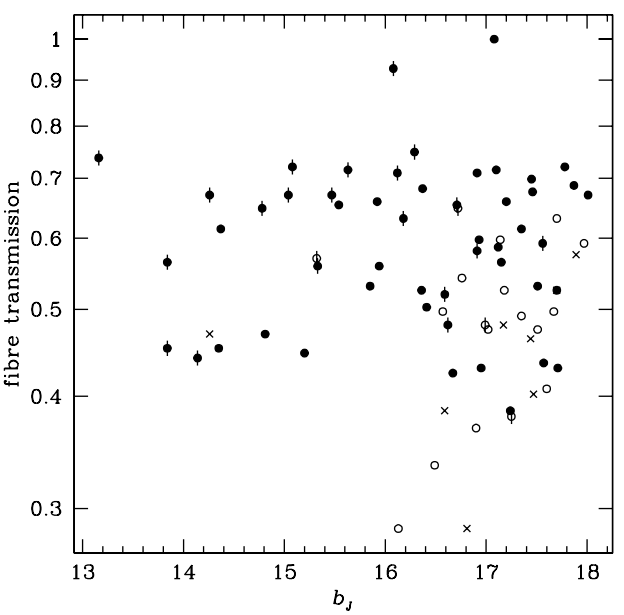

Figure 3 Fibre response (normalised to max = 1) versus blue magnitude for field F787. Same symbols as in Figure 1.

18 additional failures for exposures as short as 4000 s all involved fibres whose transmission was less than 65% of that of the best fibre. In other words, all fibres with transmissions above 65% of the nominal (best) value produced 100% redshift success in field F787.

Figure 4 shows the absolute magnitudes in B and J versus radial velocity. The figure highlights two galaxies with overestimated fluxes in the B band, the more luminous one representing, at face value, a 40 L_* galaxy, classified as a star in the COSMOS, thus confirming the misclassifications and flux overestimation of bright galaxies in COSMOS (see Section 4.2 above).[5]

The rate of overall successful redshift measurement obtained for field F787 from a 2×2000 s combined integration was a modest 69% to $b_J < 17.5$ increasing to 90%

[5]The spectrum of this object, F787–33, was of good quality, as attested by its large R and small δv in Table 2.

https://doi.org/10.1071/AS01041 Published online by Cambridge University Press

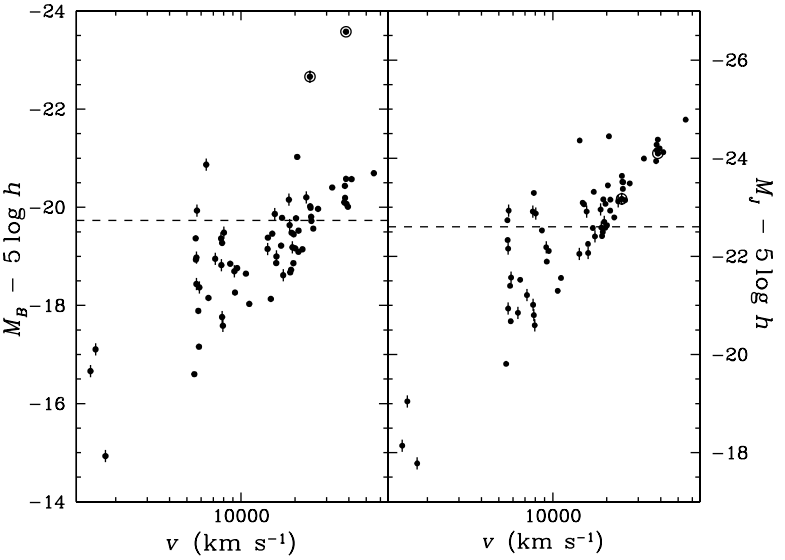

Figure 4 Absolute magnitude versus radial velocity for field F787 in bands b_J (*left*) and J (*right*). *Circles with vertical bars*: galaxies with emission lines. The two galaxies with very bright B band absolute magnitudes are shown as *surrounded circles*. The *dashed lines* represent the exponential cutoff of Schechter functions: $M_B^* = -19.73 + 5 \log h$ (Folkes et al. 1999) and $M_J^* = -22.6 + 5 \log h$ (eq. [1] below), where $h = H_0/(100\,\mathrm{km\,s^{-1}\,Mpc^{-1}})$.

Table 5. Redshift success rates for 44 ks exposures in field F20

$J^{\rm lim}$	N	P(success)	$b_J^{\rm lim}$	N	P(success)
13.0	5	0.40 ± 0.35	17.0	7	0.43 ± 0.29
13.3	8	0.38 ± 0.28	17.5	10	0.40 ± 0.24
13.6	16	0.50 ± 0.18	18.0	24	0.42 ± 0.16
13.9	29	0.41 ± 0.14	18.5	27	0.44 ± 0.14

Notes: $J^{\rm lim}$ and $b_J^{\rm lim}$ are limiting magnitudes in the NIR J and optical b_J wavebands, respectively. N represents the total number of targeted objects within the given limiting magnitude. P(success) is the probability of successful galaxy redshift measurement, i.e. the fraction of targeted objects that led to non-stellar redshifts. Note that three objects had no COSMOS counterparts, hence no optical magnitude. The error bars are binomial.

with a combined field dwell time of 17 000 s. This compares with up to 95% redshift success reported in the FLAIR manual (Parker 1995; Parker & Watson 1995) for a COSMOS B selected sample to $b_J < 17.5$ in 2000 s, admittedly obtained immediately after the system had been overhauled and cleaned. The 4000 s integration times are about what is envisaged for the 6dFGRS to achieve the expected survey productivity and completeness. Note that the NIR selection did not degrade the rate of redshift success. Indeed, Table 4 indicates a rate of success at $J \leq 13.9$, similar to that of the comparable depth $b_J \leq 17.5$ (the median $b_J - J$ for our high latitude F787 sample with $J \leq 13.9$ is 3.51).

The efficiency of redshift measurements was much worse for the galaxies in the low galactic latitude F20 field. For field F20, among 33 candidate galaxies, only 30 were fibred, while two objects were bright stars (as seen from inspection of the UKST plate) and one had a detached fibre. Among the 30 spectra, 13 yielded redshifts, one of

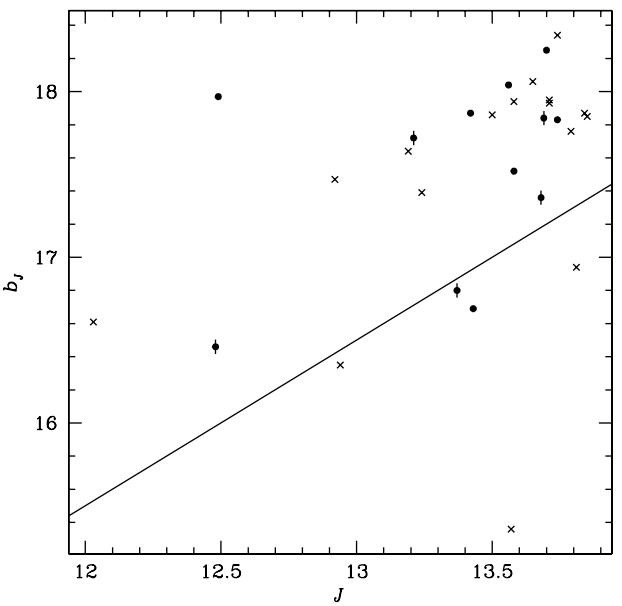

Figure 5 Same as Figure 1 for the low galactic latitude field F20. The line represents again $b_J - J = 3.5$ (the median colour at high galactic latitude) to allow comparison with Figure 1.

which turned out to be a star. As shown in Table 5, at all limiting magnitudes less than half of the targets yielded galaxy redshifts for observations as long as 44 ks. This low efficiency is partly due to the increased extinction in the field. Indeed, the median $b_J - J$ is 4.22 for the 29 candidate galaxies, in comparison with a median of 3.51 for the 69 galaxies targeted in field F787, suggesting $E(b_J - J) = 0.7$, which translates into $A_V \simeq 0.75$.

Figure 5 illustrates the efficiency of FLAIR II for the F20 field. The figure indicates that most (but not all) failures of redshift measurements are among red, optically

https://doi.org/10.1071/AS01041 Published online by Cambridge University Press

faint ($b_J > 17.5$) galaxies that suffer from high extinction. All the counterexamples (except one at $b_J = 17.5$) have transmissions lower than 55% of the maximum of the fibres of field F787, so that redshift failures in field F20 appear to be a combination of extinction and poor fibre transmission.

The lower than expected performance of FLAIR II overall can be partially explained by the generally poor seeing and intermittent cloud during the observation nights adversely affecting the signal-to-noise ratio. However, Figure 3 strongly suggests that the main culprit was a general decrease in the fibre responses. The patchy degradation of the overall fibre transmissions and the observed wide range in fibre–fibre transmission variations compared to what has been previously reported for FLAIR II is a known effect associated with the gradual degradation in the transmission of the optical cement used to bond prism to fibre, caused by the continual high UV illumination of the fibre–cement–prism interface when gluing the fibres in position over the target objects (Lee 1995). These data were taken at the end of the refurbishment cycle, shortly after which FLAIR II was converted to an intermediate magnetic button system as a preliminary test-bed for 6dF, and all ferrules had their prism–cement–fibre interfaces cleaned and re-done. Significantly improved fibre–fibre transmission consistency was obtained together with a recovery in overall fibre transmission. These improvements bode well for 6dF. Nevertheless, high extinction low galactic latitude fields will require considerably longer exposure times, and the factor of $44\,200/17\,400 = 2.5$ is clearly insufficient.

4.4 Emission Line Galaxies

An interesting aspect of NIR selected galaxy samples is that they are not biased to star forming emission line galaxies (hereafter, ELGs). It is therefore interesting to know what fraction of a NIR selected sample is composed of ELGs.

Figure 1 shows that the ELGs in the high galactic latitude F787 field, represented by vertical bars, are more frequent in brighter galaxies in the b_J band, but more spread out in J magnitude. The different trend between optical and NIR bands simply reflects the blue colours of emission line galaxies. This is illustrated in Figure 6, which shows that ELGs are roughly 0.5 magnitude bluer than galaxies with no emission lines (hereafter, NELGs) of the same absolute magnitude.

Table 6 shows the resulting fractions of ELGs in various J magnitude limited subsamples of field F787. For our largest complete magnitude limited sample at $J \leq 13.9$, we have $37 \pm 6\%$ of emission line spectra among our galaxies with measured redshifts. This fraction can be compared to the 30% of emission line spectra in a spectroscopic followup of 2MASS galaxies, selected at $K \leq 12.2$ (J. P. Huchra 1999, private communication). In comparison, over 60% of galaxies selected from two optical samples of comparable depth (the $b_J < 17.0$ Durham–UKST and the $b_J < 17.5$ Stromlo–APM galaxy catalogues) display Hα in emission (Ratcliffe et al. 1998; Tresse et al. 1999).

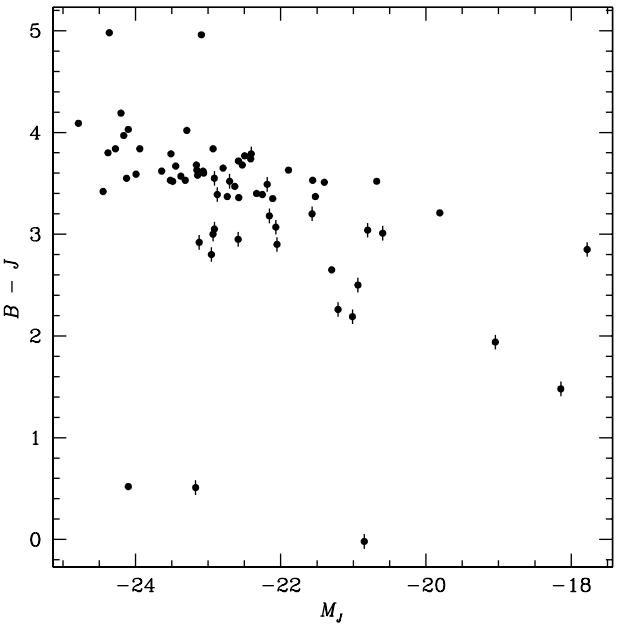

Figure 6 Colour–luminosity diagram for field F787. Emission line galaxies are the *symbols with vertical bars*. Note that the three objects with $b_J - J < 1$ are galaxies classified as stars by COSMOS.

Table 6. Fraction of emission line galaxies vs. apparent magnitude (field F787)

$J^{\rm lim}$	N	Fraction	$b_J^{\rm lim}$	N	Fraction
12.1	9	0.56 ± 0.17	15.0	9	0.67 ± 0.16
12.4	12	0.50 ± 0.14	15.5	15	0.73 ± 0.11
12.7	16	0.50 ± 0.12	16.0	20	0.60 ± 0.11
13.0	22	0.41 ± 0.10	16.5	29	0.55 ± 0.09
13.3	29	0.41 ± 0.09	17.0	42	0.52 ± 0.08
13.6	40	0.38 ± 0.08	17.5	56	0.41 ± 0.07
13.9	63	0.37 ± 0.06	18.0	68	0.35 ± 0.06

Note: The error bars are binomial.

In the low galactic latitude F20 field, one may expect that selection effects caused by extinction would lead to a different fraction of ELGs. However, the fraction of ELGs in field F20 is $42 \pm 14\%$, consistent with that in the high galactic latitude field F787.

Figure 4 shows how the ELGs are distributed in absolute magnitude and redshift for field F787. There is a clear trend towards a larger fraction of ELGs for less luminous galaxies. This is quantified in Table 7.

Figure 7 shows the distribution of absolute J magnitudes in field F787. A Wilcoxon rank-sum test indicates over 97% probability that the J band luminosities of ELGs are, on average, lower than those of NELGs. A qualitatively similar trend of increasing fraction of ELGs with decreasing luminosity has been reported by Tresse et al. (1999) for the optically selected Stromlo–APM sample. Compared to the optical, one expects a stronger trend

https://doi.org/10.1071/AS01041 Published online by Cambridge University Press

Table 7. Fraction of emission line galaxies vs. absolute J magnitude (field F787)

M_J	N	f
–25 to –24	10	0.00 ± 0.00
–24 to –23	18	0.11 ± 0.07
–23 to –22	24	0.50 ± 0.10
–22 to –17	17	0.59 ± 0.12

Notes: The error bars are binomial.

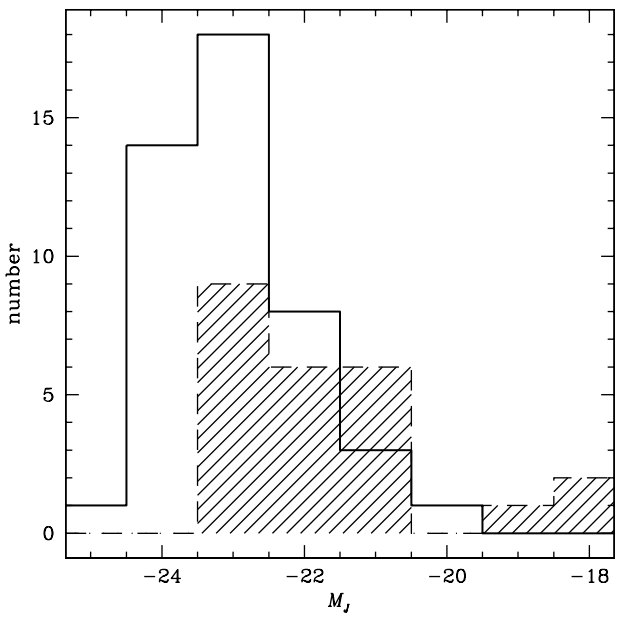

Figure 7 Distribution of absolute J magnitudes for galaxies in field F787 with (*shaded dashed histogram*) and without (*solid histogram*) emission lines.

of ELG fraction versus absolute magnitude in the NIR, because ELGs are intrinsically blue (see Figure 6).

4.5 Luminosity Function

We have attempted to evaluate the J band galaxy luminosity function for the 63 galaxies with $J \leq 13.9$ of the high galactic latitude field F787, using the simplest methods given in Willmer (1997). Because of the small number of galaxies, we restrain ourselves to the STY (Sandage, Tammann & Yahil 1979) parametric, maximum likelihood estimator, assuming a Schechter (1976) luminosity function $\phi(L) = \phi_*/L_* \, (L/L_*)^\alpha \, \exp(-L/L_*)$.

Neglecting magnitude and redshift errors, as well as Galactic extinction and the k terms (indeed, $|k_J| \leq 0.1$ for $z \leq 0.2$ as in our sample, see Poggianti 1997; Mannucci et al. 2001), and assuming $\Omega_m = 0.3$ and $\Omega_\Lambda = 0.7$ (for the luminosity distances required to convert apparent to absolute magnitudes), we derive reasonable maximum likelihood parameters

$$\alpha = -1.1 \pm 0.4 \qquad M_J^* = -22.6 \pm 0.5 + 5 \log h, \quad (1)$$

where the errors are 68% confidence constant likelihood contours equal to the maximum likelihood value offset by the usual $0.5 \, f_{\chi^2}(2)$.[6]

We evaluated the normalisation of the luminosity function using the relation (e.g. Willmer 1997, Section 3) $\phi_* = \bar{n} / \int_{M_{\rm bright}}^{M_{\rm faint}} \phi(M) \, dM$, where $\bar{n}$ is the number density of galaxies (corrected for the selection function, see Willmer 1997, equation [33]), evaluated in 10 velocity bins out to 35 000 km s^{-1} (beyond which our data is too sparse). We obtain

$$\phi_* = 0.010^{+0.0052}_{-0.0035} \, h^3 \, {\rm Mpc}^{-3}, \quad (2)$$

where the uncertainty is estimated from the uncertainty of $\bar{n}$ (thus neglecting the uncertainties in α and M_J^*).

Our luminosity function parameters (equations [1] and [2]) match well those of Cole et al. (2001), and our slope α and normalisation ϕ_* also match very well that of the optical Stromlo–APM survey (Loveday et al. 1992).

4.6 Large-scale Structure

Figure 8 shows the resulting wedge diagrams for field F787. Note that these wedges are incomplete, as only 11 out of 35 possible DENIS strips covered the UKST F787 field. One notices galaxy concentrations at radial velocities near 20 000 and 38 000 km s^{-1}, the first of which includes a galaxy that lies within 42″ of the Abell 1434 cluster, whose redshift is not yet known.

Our measurement based upon a single, possibly interloping object gives a tentative $z = 0.0686$ for Abell 1434. If Abell 1434 lies at that distance, an angle of 42″ corresponds to a physical separation of $42 \, h^{-1}$ kpc, which would place object F787–37 at the core of the cluster.

Inspection of Figure 8 indicates that the concentration at 38 000 km s^{-1} is for a fairly constant Dec and a range of RAs, corresponding to a comoving scale of $11 \, h^{-1}$ Mpc, indicative of a supercluster.

Figure 9 shows the resulting wedge diagrams for field F20. Concentrations are apparent at $cz = 12\,000$ and 22 000 km s^{-1}.

5 Conclusions

This pilot study for the forthcoming 6dFGRS has provided useful information on various aspects of the survey. First, it has shown that the preliminary galaxy extraction from DENIS images was highly reliable, even at low galactic latitudes ($b = -17°$), where the reliability, based upon subsequent visual inspection of photographic plates, was 93%, despite confusion with double stars and extinction. Second, it pointed to a degraded fibre transmission, which has been attended to since. Also a newly commissioned 1K EEV CCD for 6dF is expected to significantly

[6] C. Willmer kindly checked our luminosity function for us, and furthermore ran Monte Carlo simulations of magnitude limited galaxy distributions with 63 members, derived from a parent Schechter luminosity function to check that the uncertainty in the STY estimate of the parameters was of the order of the error bars quoted in equation (1).

https://doi.org/10.1071/AS01041 Published online by Cambridge University Press

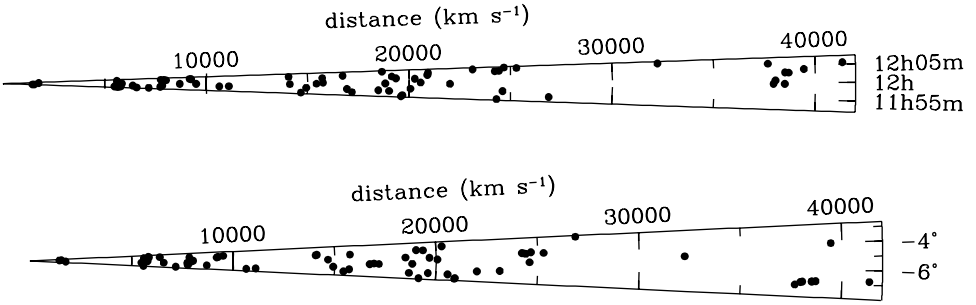

Figure 8 Wedge diagrams for field F787. One galaxy lies at $v = 55\,000\,\mathrm{km\,s^{-1}}$.

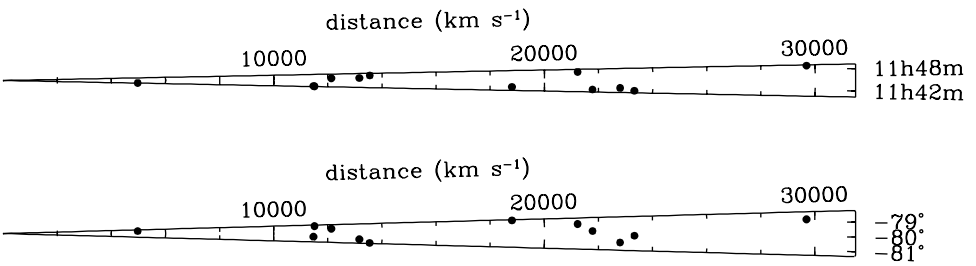

Figure 9 Wedge diagrams for field F20. These wedges are narrower than in field F787, because no DENIS strips were available near the plate edges.

improve the instrument throughput. Third, it proved that optical spectroscopy of high latitude, NIR-based samples is feasible with similar rates of successful redshift measurement as in optically selected galaxy samples. Fourth, it indicated that redshifts can be obtained at low galactic latitude, although with much less success than at high galactic latitude.

There are therefore good reasons to have full confidence in the success of the 6dFGRS in obtaining a highly complete redshift followup of galaxies selected in the NIR by 2MASS and DENIS, although this success may be limited to high galactic latitudes. Note that the primary sample of 6dFGRS will be the longer wavelength K_s band at 2.15 μm, and there is expected to be a larger fraction of galaxies with only absorption lines, for which redshifts are generally harder to measure.

Moreover, our study has provided a first estimate on the fraction of emission line galaxies in a J band selected galaxy sample and its variation with galaxy J band luminosity, as well as an estimate of the J band galaxy luminosity function. Serendipitous results include a tentative redshift for the Abell 1434 cluster as well as the establishment of various concentrations of galaxies, including a possible supercluster at $380\,h^{-1}$ Mpc.

Acknowledgements

We warmly thank Malcolm Hartley for operating the UKST telescope, Paul Cass for fibering one of the plates, and Matthew Colless and Brian Boyle for useful discussions and encouragement. We are very grateful to Chris Willmer who checked our luminosity functions and ran Monte Carlo simulations to check the error estimates. We also thank Santiago Arribas and a second anonymous referee for useful comments on the manuscript. These observations were based upon images taken by the DENIS NIR imaging survey, which is supported in France by the Institut National des Sciences de l'Univers, the Education Ministry and the Centre National de la Recherche Scientifique, in Germany by the State of Baden-Würtemberg, in Spain by the DG1CYT, in Italy by the Consiglio Nazionale delle Ricerche, and in Austria by the Fonds zur Förderung der Wissenschaftlichen Forschung und Bundesministerium für Wissenshaft und Forschung. We are grateful to the DENIS staff, and in particular Jean Borsenberger for flat-fielding the DENIS images, and Emmanuel Bertin for help with the SExtractor source extraction package. GAM acknowledges a travel grant from the Coopération France–Australie. We made use of the ROE/NRL COSMOS UKST Southern Sky Object Catalogue, the Digitized Sky Survey produced at the Space Telescope Science Institute under US Government grant NAG W-2166, and the NASA/IPAC Extragalactic Database (NED), which is operated by the Jet Propulsion Laboratory, California Institute of Technology, under contract with the National Aeronautics and Space Administration.

References

Bertin, E., & Arnouts, S. 1996, A&AS, 117, 393
Cole, S. et al. 2001, MNRAS, 326, 255

https://doi.org/10.1071/AS01041 Published online by Cambridge University Press

Epchtein, N. et al. 1999, A&A, 349, 236
Folkes, S. et al. 1999, MNRAS, 308, 459
Héraudeau, P., Simien, F., & Mamon, G. A. 1996, A&AS, 117, 417
Jarrett, T. H., Chester, T., Cutri, R., Schneider, S., Skrutskie, M., & Huchra, J. P. 2000a, AJ, 119, 2498
Jarrett, T. H., Chester, T., Cutri, R., Schneider, S., Rosenberg, J., Huchra, J. P., & Mader, J. 2000b, AJ, 120, 298
Kron, R. G. 1980, ApJS, 43, 305
Kurtz, M. J., & Mink, D. J. 1998, PASP, 110, 934
Lee, S. 1995, AAO internal report
Loveday, J., Peterson, B. A., Efstathiou, G., & Maddox, S. J. 1992, ApJ, 390, 338
Mamon, G. A. 1998, in Wide Field Surveys in Cosmology, ed. S. Colombi, Y. Mellier, & R. Raban (Paris: Frontières), 323 (astro-ph/9809376)
Mamon, G. A. 2000, in Cosmic Flows 1999: Towards an Understanding of Large-Scale Structure, ed. S. Courteau, M. A. Strauss, & J. A. Willick (San Francisco: ASP [vol. 201]), 103 (astro-ph/9908163)
Mamon, G. A., Borsenberger, J., Tricottet, M., & Banchet, V. 1998, in The Impact of Near-Infrared Sky Surveys on Galactic and Extragalactic Astronomy, ed. N. Epchtein (Dordrecht: Kluwer), 177 (astro-ph/9712169)
Mannucci, F., Basile, F., Poggianti, B. M., Cimatti, A., Daddi, E., Pozzetti, L., & Vanzi, L. 2001, MNRAS, 326, 745
Parker, Q. A. 1995, Spectrum, 7, 17
Parker, Q. A., & Watson, F. G. 1995, in Wide Field Spectroscopy and the Distant Universe, ed. S. J. Maddox (Singapore: World Scientific), 33
Parker, Q. A., Watson, F. G., & Miziarski, S. 1998, in Fiber-Optics in Astronomy III, ed. S. Arribas, E. Mediavilla, & F. Watson (San Francisco: ASP [vol. 152]), 80
Poggianti, B. M. 1997, A&AS, 122, 399
Ratcliffe, A., Shanks, T., Parker, Q. A., Broadbent, A., Watson, F. G., Oates, A. P., Collins, C. A., & Fong, R. 1998, MNRAS, 300, 417
Sandage, A., Tammann, G. A., & Yahil, A. 1979, ApJ, 232, 352
Schechter, P. 1976, ApJ, 203, 297
Tonry, J., & Davis, M. 1979, AJ, 84, 1511
Tresse, L., Maddox, S. J., Loveday, J., & Singleton, C. 1999, MNRAS, 310, 262
Watson, F. G., Parker, Q. A., Bogatu, G., Farrell, T. J., Hingley, B. E. & Miziarski, S. 2000, SPIE, 4008, 123
Willmer, C. N. A. 1997, AJ, 114, 898
Zaritsky, D., Rix, H.-W., & Rieke, M. 1993, Nature, 364, 313

https://doi.org/10.1071/AS01041 Published online by Cambridge University Press